Proceedings of ASME Turbo Expo 2011
GT2011
June 6-10, 2011, Vancouver, British Columbia, Canada

GT2011-45151

PROBABILISTIC HIGH-CYCLE FATIGUE RISK ASSESSMENT OF AN INTEGRALLY BLADED ROTOR

Benjamin D. Hall
HCF & Stage Vibrations
Pratt & Whitney
East Hartford, Connecticut 06108
Email: benjamin.hall@pw.utc.com

Lauren Gray
Fatigue & Fracture Mechanics
Pratt & Whitney
East Hartford, Connecticut 06108
Email: lauren.gray@pw.utc.com

ABSTRACT

A fully probabilistic high-cycle fatigue (HCF) risk assessment methodology for application to turbine engine blades is described. The assessment uses the Bayesian paradigm of probability theory in which probability distributions are used to encode states of knowledge. Multi-level (or hierarchical) models are employed to capture engineering knowledge of the factors important for assessing HCF risk. This structure allows us to use standard probability distributions to adequately represent uncertainties in model parameters. The model accounts for engine-to-engine, run-to-run, and blade-to-blade variability as well as uncertainty in material capability, usage (flight conditions, time at resonance), and steady and vibratory stresses. Markov chain Monte Carlo (MCMC) simulation is used to fit observed data to the engineering models, then direct Monte Carlo simulation is used to assess the HCF risk.

INTRODUCTION

Turbine engine airfoil high cycle fatigue (HCF) failures have been a systemic issue for all turbine engine manufacturers and operators. High cycle fatigue results from vibratory stress cycles induced by various aeromechanical sources, and has led to the premature failure of major engine components with substantial cost and readiness impacts. New probabilistic-based tools and validation strategies that recognize both the uncertainty of, and inherent variability in manufactured part, component and engine geometries, material capability, and usage, are needed now to ensure the success of future lightweight, robust and competitive designs.

One such process for applying probabilistic methods to assess HCF risk in the validation phase of engine development is discussed. The probabilistic HCF risk assessment augments the deterministic Goodman assessment by explicitly modeling and quantifying the uncertainties in steady stress, vibratory stress, and capability. In most cases, the deterministic Goodman-based approach is an effective means for quantify HCF risk. The proposed approach improves the quantification of HCF risk in certain situations.

The approach is based on the Bayesian paradigm of probability theory because it provides a unified, logical, and rationally consistent approach to reasoning in the presence of uncertainty. Laplace [1] was the first to employ the theory in a way that could be appreciated by modern engineers and scientists. His work was augmented by Jeffreys [2], Cox [3], and Jaynes [4]. More recent scientific and engineering-based introductions to Bayesian probability theory and its applications include the works of Bretthorst [5], Sivia [6], and Gregory [7]. Advancements in hierarchical models and Markov chain Monte Carlo computation as described by Gilks, et al. [8], Gelman, et al. [9], Gelman and Hill [10] and Liu [11] have made it practical to analyze more sophisticated probabilistic models.

LEGACY APPROACH

The legacy process for HCF validation compares a worst-case vibratory stress to a conservative measure of the material capability. The limiting stresses are identified and plotted on a

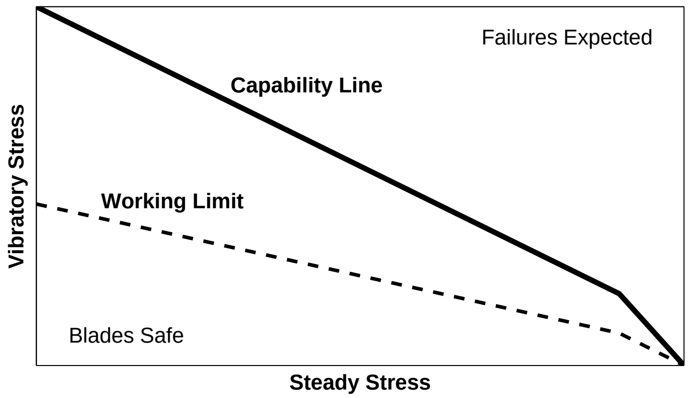

FIGURE 1. EXAMPLE GOODMAN DIAGRAM FOR DETERMINISTIC VALIDATION.

Goodman diagram [12]; a simple example is shown in Fig. 1. When the responses are below the working limit, the design is acceptable. Conversely, when stresses are observed at levels exceeding the Goodman criteria the design must be improved.

PROBABILISTIC APPROACH

In practice, it is not uncommon for a few observed responses to be near to the allowable working limit. The probabilistic approach described herein is intended to be used for these responses to more accurately quantify HCF risk.

The major elements of the probabilistic HCF risk assessment are a: damage accumulation model, component capability model, usage model, steady stress model, and vibratory stress model. The elements fit together as shown in Fig. 2 to calculate the probability of a failure due to high cycle fatigue. The calculated failure probability is compared to an allowable limit to determine acceptability of the design.

Probability distributions are used to describe states of knowledge. The notation $p(A|BI)$, read the probability of A given B and I, characterizes the state of knowledge regarding the plausible values for the proposition A. The vertical bar in $p(A|BI)$ is referred to as the conditioning bar and all quantities to the right of it are assumed true, or given as known, when assessing the probability of propositions. Following the lead of Jeffreys [2] and Jaynes [4] the symbol I is included in the conditioning list of all probability statements. This is used to represent all the other information that defines the problem and led to the current formulation. It serves as a reminder that no probabilities are absolute.

Cox [3] demonstrated that the simple rules of probability theory are the uniquely valid principles for ensuring rational and logically consistent reasoning in the presence of uncertainty.

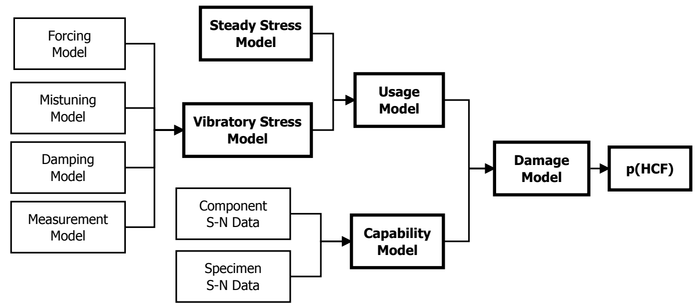

FIGURE 2. MAJOR ELEMENTS OF THE PROBABILISTIC HCF RISK ASSESSMENT.

These rules are the sum rule

$$p(A|I) + p(\overline{A}|I) = 1$$

and product rule

$$p(AB|I) = p(A|I)p(B|AI) = p(B|I)p(A|BI)$$

where the value 0 denotes impossibility and the value 1 certainty. The notation $\overline{A}$ is the negation (or denial) of the proposition A; Tribus [13] discusses the value of explicitly formulating the denial statement $\overline{A}$ for each proposition A.

Bayes' theorem is obtained immediately from the product rule of probability theory

$$p(B|AI) = \frac{p(B|I)p(A|BI)}{p(A|I)}$$

and is frequently expressed as $p(B|AI) \propto p(B|I)p(A|BI)$. In a typical scenario, B is a proposition describing a hypothesis and A a proposition representing the data. Then Bayes' theorem quantifies $p(B|AI)$, the posterior probability for the hypothesis B, as proportional to the prior (to observing the data) probability $p(B|I)$ and the sampling distribution for the data $p(A|BI)$ (also known as the likelihood function for B). The sum and product rules (including Bayes' theorem) are applied repeatedly to derive the posterior distributions for the parameters of interest. The works of Sivia [6] and Gregory [7] are two recent, scientifically-oriented introductions to probability theory as employed herein.

REQUIREMENTS

Specific requirements must be worked out with the appropriate government agencies. The Engine Structural Integrity Program (ENSIP) handbook, MIL-HBDK-1783B [14] recommends[1] that "The probability of failure due to high cycle fatigue (HCF) for any component within or mounted to the engine should be below 1x10-7 per engine flight hours (EFH) on a per-stage basis, provided the system-level safety requirements are met." Similarly, the Federal Aviation Administration (FAA) regulations specify allowable failure rates for engine-related failures in Section 33.75 (FAR 33.75 [15]). The allowable rates depend on the severity of the failure; "hazardous engine effects" must demonstrate a rate less than 10^{-7} to 10^{-9} failures per engine flight hour with a clause indicating that "compliance may be shown by demonstrating that the probability of a hazardous engine effect arising from an individual failure can be predicted to be not greater than 10^{-8} per engine flight hour."

p(HCF) CALCULATION

For each occurrence of a resonance in the probabilistic assessment, an exposure based on predicted stresses, duration, and capability is calculated. As more events are accumulated, the exposure grows and the probability of fracture increases.

After simulating an entire engine lifetime and assessing the probability of fracture for each blade in the wheel, the results are combined to determine the overall risk of fracture for the stage. If multiple failure modes are of concern the results from each are again combined. The entire process is repeated to assess the overall risk of a fleet.

For each engine:

- Select a blade set (room temperature frequencies), $f_{r,b}$ from Eqn. (3).
- Calculate blade mistuning pattern, $\{\alpha\}$.
- Select forcing model parameters, $\sigma_v^{(i)}, v_0^{(i)}, A^{(i)}$ from the MCMC sample, Eqn. (9).
- For each blade:
  - Select material model parameters (S-N curves), $A^{(i)}, B^{(i)}, \sigma_N^{(i)}$ from the MCMC sample, Eqn. (12).
  - Select "nominal" steady stress value, s_0 from Eqn. (1).
- For each mission (and blade):
  - Identify / select performance parameters
  - Calculate resonant frequency and crossing speed (adjusted by temperature), Eqn. (2).
  - Calculate speed-squared adjustment for steady stress, Eqn. (4).
  - Calculate vibratory stress from the forcing model, Eqn. (8).
  - Calculate exposure based on blade frequency and time at resonance, Eqn. (14)
  - Update cumulative exposure, Eqn. (15).

[1]The handbook is for guidance only and is not to be cited as a requirement.

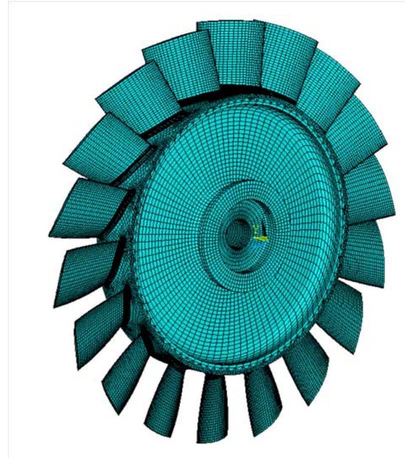

FIGURE 3. FINITE ELEMENT MODEL OF PURDUE IBR USED FOR DEMONSTRATING PROBABILISTIC HCF RISK ASSESSMENT PROCESS.

Calculate probability of failure for each blade, Eqn. (17).

Calculate probability of failure for stage, Eqn. (18).

Calculate the fleet risk, Eqn. (19).

Example Application

The discussion is presented in terms of the "Purdue" integrally-bladed rotor (IBR), a test article with 18 blades which was part of the GUIde program [16, 17]. A finite element model of the IBR is shown in Fig. 3. The analysis is based on hypothetical strain gage data for a 24 count (24E) vane-pass excitation of the fifth airfoil-dominated, second torsion (2T) mode. Lab test data from two IBRs identifies the mean and standard deviation of the mode frequency as 8070 Hz and 100 Hz, respectively.

Steady Stress Model

The steady stress (at resonance) model is composed of two pieces. First is a distribution of "nominal" steady stresses that are expected as a result of the within-tolerance geometric variations of the blades. Second is a model that describes how the steady stress varies with crossing speed. This latter model accounts for both the influence of temperature on resonant crossing speed as well as the natural scatter in the as-manufactured blade frequencies.

The deterministic model for the steady stress at resonance is $s = s_0(N/N_0)^2$ where s_0 is the steady stress at the nominal resonance speed N_0 and N is the actual resonance speed. Based on finite element analyses of various, within-tolerance geometric data, a Gaussian distribution for the nominal steady stress s_0 is identified

$$p(s_0|\mu_{s_0},\sigma_{s_0},I) = \frac{1}{\sqrt{2\pi}\sigma_{s_0}}\exp\left[-\frac{(s_0-\mu_{s_0})^2}{2\sigma_{s_0}^2}\right] \quad (1)$$

where μ_{s_0} is the expected value and σ_{s_0} the standard deviation of stress.

The relationship $f = EN/60$ is used to calculate the resonant speed N (in revolutions per minute) given the engine-order excitation E (in cycles per revolution) and the frequency of vibration f (in Hz). The dependence of frequency on temperature is modeled as

$$f = f_r + A(T - T_r) \quad (2)$$

where T is a temperature (e.g., inlet temperature), T_r a reference temperature (such as standard day), A a constant, assumed known for the present analysis, and f_r the frequency at the reference temperature.

In this model, only the reference frequency is treated as uncertain and modeled with a Gaussian distribution

$$p(f_r|\mu_{f_r},\sigma_{f_r},I) = \frac{1}{\sqrt{2\pi}\sigma_{f_r}}\exp\left[-\frac{(f_r-\mu_{f_r})^2}{2\sigma_{f_r}^2}\right] \quad (3)$$

where the mean μ_{f_r} and standard deviation σ_{f_r} are estimated from lab test data; both are treated as known with certainty in the present analysis. The principle of maximum entropy [4, 6, 7, 18, 13] shows that the Gaussian distribution is one that makes a minimal number of assumptions regarding the possible values of an unknown quantity and one that is frequently consistent with what is known before data are collected. Furthermore, the Gaussian distribution is a good description of the observed data.

The conditional probability distribution for steady stress at resonance is

$$p(s|s_0,f_r,A,T,T_r,f_0,I) = \delta\left(s - s_0\left[\frac{f_r + A(T-T_r)}{f_0}\right]^2\right) \quad (4)$$

where $\delta(x)$ is the Dirac delta function. This probability distribution says that, given the value of all of the parameters to the right of the conditioning bar, the value of stress is unambiguously defined. See Bretthorst [19] or Tribus [13] for more information on using delta functions as a means of incorporating deterministic statements into a probability formulation.

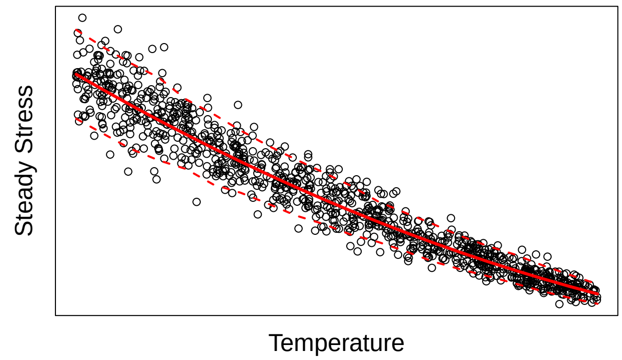

FIGURE 4. SIMULATED VALUES FROM THE STEADY-STRESS MODEL (DOTS) ALONG WITH THE MEAN (SOLID LINE) AND 90% RANGE (DASHED LINES).

To determine the range of plausible stress values at any given temperature, the nominal stress s_0 and the frequency f_r of individual blades are nuisance parameters and eliminated through marginalization. This gives

$$\begin{aligned} p(s|T,\theta,I) &= \iint p(ss_0f_r|T,\theta,I)\,ds_0\,df_r \\ &= \iint p(s_0|\theta I)p(f_r|\theta I)p(s|s_0,f_r,T,\theta,I)\,ds_0\,df_r \end{aligned} \quad (5)$$

where $\theta = \{E,A,T_r,f_0,\mu_{s_0},\sigma_{s_0},\mu_{f_r},\sigma_{f_r}\}$ is short-hand for the model parameters taken as known in the present analysis. A numerical approximation is obtained via Monte Carlo integration as

$$\hat{p}_m(s|T\theta I) = \frac{1}{m}\sum_i p(s|s_0^{(i)}f_r^{(i)}T\theta I)$$

where $s_0^{(i)}$ and $f_r^{(i)}$ are independent draws from Eqn. (1) and Eqn. (3) and the distribution appearing in the summation is Eqn. (4). For more details on Monte Carlo integration, consult the works of Liu [11] or Robert and Casella [20].

An example of draws from the distribution Eqn. (5) of steady stress as a function of temperature is shown in Fig. 4. The black dots are the simulated values and the red lines show the mean and 90% range of the data as a function of temperature. To highlight some of the interesting features of the model some of the parameter values were artificially set to unrealistic values (the values used were $E = 24, A = -17, T_r = 70, f_0 = \mu_{f_r}, \mu_{s_0} = 50, \sigma_{s_0} = 5, \mu_{f_r} = 8070, \sigma_{f_r} = 100$) for the figure.

Vibratory Stress Model

The vibratory stress model is composed of mistuning and nominal-blade forced-response sub-models. A distribution of predicted stresses is produced that includes blade-to-blade, run-to-run, and engine-to-engine variability. The form of the vibratory stress model is motivated by linear vibration theory [21] which specifies that the peak vibratory stress μ_v in a resonant response is given by

$$\mu_v \propto \frac{\phi^T F}{2\zeta} \tag{6}$$

where ϕ is the mode shape, F the unsteady forcing, and ζ the damping ratio. The notation ϕ^T represents the transpose of the mode shape vector ϕ.

Small, within-tolerance geometric variations of airfoils can cause significant variation in the individual blade mode shapes and hence peak vibratory stresses [22, 23]. Presently, this mistuning is modeled as $\phi_b = \alpha_b \phi_0, b = 1, 2, \ldots, 18$, where ϕ_b is the mode shape of blade b, α_b is a mean-normalized mistuning scale factor and ϕ_0 is the nominal mode shape. The forced-response amplitude of each blade b is obtained by substituting ϕ_b for ϕ into Eqn. (6). The mistuned mode shape is a property of the structure and does not vary with usage.

The forcing F is the same for all blades, but varies with operating condition. For the present example, a linear relationship between forcing amplitude and pressure is sufficient. The forcing model is $F = \beta^*(p)F_0$ where F_0 is the nominal forcing "shape" and $\beta^*(p)$ describes how the amplitude of the forcing varies with pressure. In practice, not only the forcing amplitude, but also the shape, or distribution of unsteady pressure across the airfoil surface, may vary with conditions.

In general, the damping ζ varies from blade-to-blade and also with conditions (e.g., pressure). Frequently, wide variations are observed in reported damping values, both between blades as well as from run-to-run. For this illustration, variations in damping are ignored and it is treated as a constant, common to all blades.

Combining all of this information results in the deterministic model

$$\begin{aligned} \mu_{v,b} &= c\alpha_b \beta^*(p) \frac{\phi_0^T F_0}{2\zeta} \\ &= \alpha_b \beta(p) \\ &= \alpha_b \left[v_0 + A(p - p_r)\right] \end{aligned} \tag{7}$$

for the expected value of the peak vibratory stress $\mu_{v,b}$ of blade b. The constants have been absorbed into the force scaling function $\beta(p) = c\phi_0^T F_0/(2\zeta)\beta^*(p)$. The Gaussian distribution is again used to describe the knowledge regarding the differences between the model predictions and the measured data to obtain the probabilistic model

$$p(v_b|\sigma_v \alpha_b v_0 A p I) = \frac{1}{\sqrt{2\pi}\sigma_v} \exp\left[-\frac{(v_b - \mu_{v,b})^2}{2\sigma_v^2}\right] \tag{8}$$

for the vibratory stress v_b of blade b with $\mu_{v,b}$ given by Eqn. (7).

The model parameters α_b (all 18 of them), v_0, A, and σ_v are estimated from the experimental data. Let $D \equiv \{(v_1, p_1), (v_2, p_2), \ldots (v_n, p_n)\}$ represent the measured pressure p_i and vibratory stress v_i data from all blades and resonant crossings collected during engine test. Further, let $\{\alpha\} = \{\alpha_1\, \alpha_2\, \ldots\, \alpha_{18}\}$ denote the set of the mistuning coefficients for each blade on the IBR obtained either from lab testing or time-of-arrival data from engine test. Assuming that the discrepancies between the model predictions and the measured responses for each data point are independent, the posterior distribution for the unknown model coefficients is

$$\begin{aligned} p\left(\sigma_v \{\alpha\} v_0 A|DI\right) \propto\; & p(\sigma_v|I)\, p(\{\alpha\}|I)\, p(v_0|I)\, p(A|I) \\ & \times \prod_i p(v_i|p_i \sigma_v \alpha_b v_0 A I). \end{aligned} \tag{9}$$

The first four quantities on the right hand side are the prior probability distributions for the model parameters and the final product represents the data likelihood.

Markov chain Monte Carlo (MCMC) analysis is used to generate simulations from the joint posterior distribution. The simulated values $\left(A^{(i)}, v_0^{(i)}, \{\alpha^{(i)}\}, \sigma_v^{(i)}\right)$ are used both to summarize the posterior distribution as well as directly in the Monte Carlo simulations of fleet risk. This ensures that the structure and all correlations of the posterior probability density are accurately captured.

Figure 5 shows example results from the analysis. The top graph is the fitted mistuned mode shape corresponding to the experimental data (that is, the values of α_b) with the error bars indicating the 95% highest posterior density interval. Note that these mistuning coefficients are only used to validate the physics-based mistuning model which is used to predict modes shapes of simulated wheels. The bottom graphs shows the marginal posterior probability densities for the parameters A and v_0. This is just one summary of the posterior distribution; a scatterplot of A versus v_0 would show the correlation of the two parameters (approximately -0.7).

Figure 6 is a plot of the measured vibratory stresses versus the model predictions for three of the observations. The full posterior distribution for the predicted stresses shown in the figure

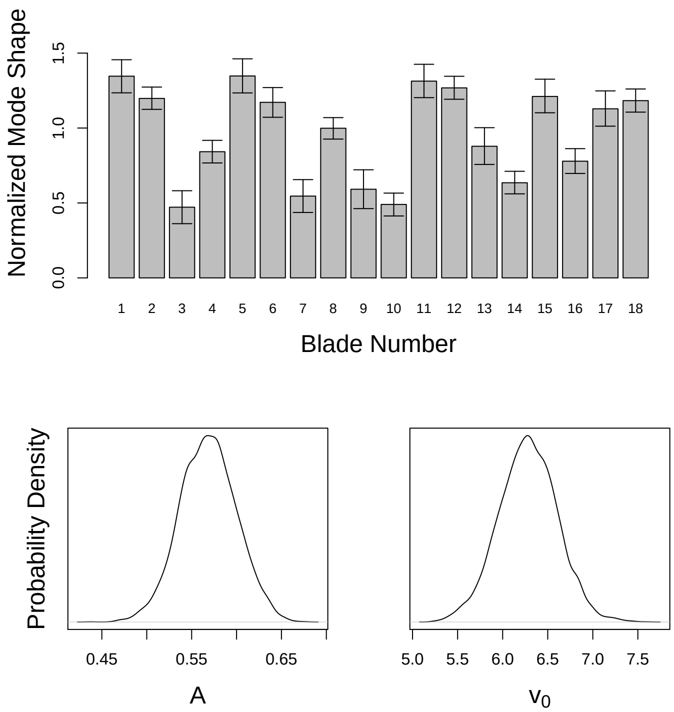

FIGURE 5. (TOP) POSTERIOR MEAN AND 95% CONFIDENCE REGION FOR MISTUNED MODE SHAPE AND (BOTTOM) MARGINAL POSTERIOR DISTRIBUTIONS FOR VIBRATORY STRESS MODEL COEFFICIENTS.

are given by

$$\begin{aligned} p(v|pDI) &= \iiiint p\,(v\sigma_v\alpha_b v_0 A|DI)\, d\sigma_v\, d\alpha_b\, dv_0\, dA \\ &= \iiiint p\,(\sigma_v\alpha_b v_0 A|DI)\, p(v|\sigma_v\alpha_b v_0 A pI) d\sigma_v\, d\alpha_b\, dv_0\, dA \end{aligned}$$

where the first term in the integral is given by Eqn. (9) and the second by Eqn. (8). Again, the integral is readily approximated with Monte Carlo integration as

$$\hat{p}_m(v|pDI) = \frac{1}{m}\sum_i p(v|\sigma_v^{(i)}\alpha_b^{(i)}v_0^{(i)}A^{(i)}pI)$$

using the MCMC simulated values from Eqn. (9).

Capability Model

The component capability model describes the stress-life (S-N) characteristics of the part across the HCF range of stresses and cycles (i.e., 10^5 cycles and above). This contrasts with the traditional approach which seeks only to describe a min-capability

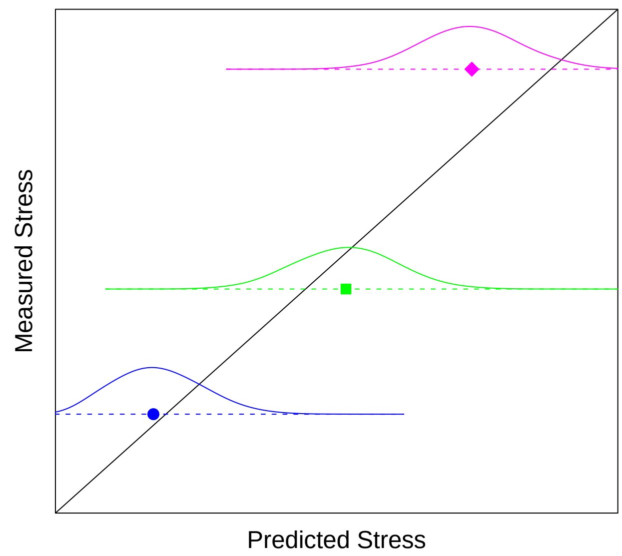

FIGURE 6. ACTUAL VERSUS PREDICTED PLOT FROM VIBRATORY STRESS MODEL.

lower bound for the strength at a specified number of cycles, usually 10^7 or 10^9, depending on the application.

The following relationship describes the correspondence between the median number of cycles to failure $\mathscr{N}$ and the applied stress level s

$$\log \mathscr{N} = A + \frac{B}{s} \tag{10}$$

The model parameters A and B are initially unknown and must be estimated from lab testing. The data D from the testing consists of n pairs of observed values $D \equiv \{(N_1, s_1), (N_2, s_2), \ldots, (N_n, s_n)\}$ and the observed cycles to failure N_i are related to Eqn. (10) by

$$\log N_i = \log \mathscr{N} + e_i.$$

where e_i is the "error" which includes both the imperfections of the data collection as well as the inadequacies of the simple assumed model. The measured stresses s_i are assumed to be known with certainty. Zellner [24] provides a comprehensive treatment of making inferences with uncertainty in both dependent and independent parameters (N and s in the present model) and discusses the limitations of what can be learned from the data alone in these situations.

The errors e_i are assumed to be logically (i.e., statistically) independent and described by a Gaussian distribution with zero mean and and standard deviation σ_N. The sampling distribution for the data that successfully initiate cracks during the S-N testing is

$$p(N_i|ABs_i\sigma_N I) = \frac{1}{N_i\sigma_N\sqrt{2\pi}} \exp\left\{-\frac{1}{2\sigma_N^2}\left[\log N_i - \left(A + \frac{B}{s_i}\right)\right]^2\right\} \tag{11}$$

which is a log-normal distribution in terms of life N. For specimens that do not initiate cracks (also called right-censored, suspensions, or runouts), the sampling distribution is

$$p(N > \tilde{N}_i|ABs_i\sigma_N I) = \int_{\tilde{N}_i}^{\infty} p(N|ABs_i\sigma_N I)dN$$

which is the area under the curve to the right of the censoring time $\tilde{N}_i$.

Direct application of the sum and product rules of probability theory provide the posterior distribution for the model parameters

$$\begin{aligned} p(AB\sigma_N|DI) \propto\ & p(A|I)p(B|AI)p(\sigma_N|I) \\ & \times \prod_i p(N_i|ABs_i\sigma_N I) \prod_{i'} p(N > \tilde{N}_{i'}|ABs_{i'}\sigma_N I) \end{aligned} \tag{12}$$

where $p(A|I)$, $p(B|AI)$, $p(\sigma_N|I)$ are the prior (to observing the data) probabilities for the model parameters, i indexes the observed failures, and i' indexes the runouts.

Markov chain Monte Carlo (MCMC) simulation is used to approximate the posterior distribution defined by Eqn. (12). The JAGS (an acronym for Just Another Gibbs Sampler) open-source software package [25] is one convenient tool for the analysis of these problems. The result of the MCMC simulation are samples of A, B, and σ_N from the joint distribution defined by Eqn. (12).

An illustration of S-N data and Bayesian analysis fits are shown in Fig. 7. The dots are the test data (open circles represent runouts). The thick black line is the best fit through the data and the thin gray lines show other plausible fits based on the posterior probability distribution for the model parameters given by Eqn. (12). In addition to visual checks, specific goodness of fit tests as described by Gelman, et al. [9] are employed to ensure that the model adequately captures the important aspects of the observed data.

Shown in Fig. 7 as blue curves are the distributions of capability at 10^7 and 10^8 cycles. The derivation of these curves follow from straight-forward application of the sum and product rules of probability theory and these curves are useful for comparisons to legacy data analyses that base Goodman curves on "min-capability" properties at a prescribed number of cycles to failure.

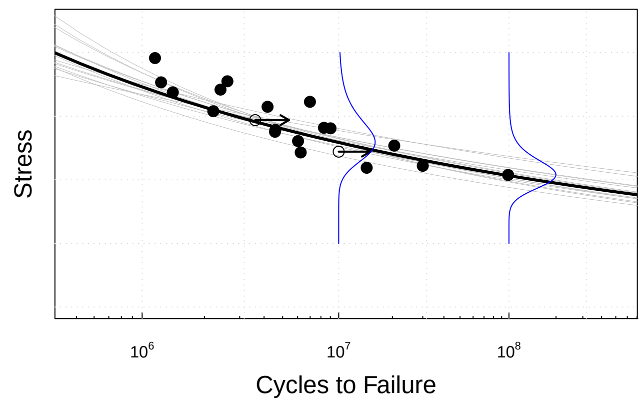

FIGURE 7. COMPONENT S-N DATA (DOTS) AND FITS TO CAPABILITY MODEL.

The posterior distribution for the number of cycles to failure at a specified stress level given all of the available information is obtained by averaging over the plausible values of the model parameters. The result is

$$\begin{aligned} p(N|sDI) &= \iiint p(NAB\sigma_N|DsI)dA\,dB\,d\sigma_N \\ &= \iiint p(AB\sigma_N|DI)p(N|sAB\sigma_N I)dA\,dB\,d\sigma_N. \end{aligned}$$

While it is difficult to further simplify the above result analytically, it is easy to approximate the integral using the MCMC simulations as

$$\hat{p}_m(N|sDI) = \frac{1}{m}\sum_{i=1}^{m} p(N|A^{(i)}B^{(i)}\sigma_N^{(i)}sI)$$

where $A^{(i)}$, $B^{(i)}$, and $\sigma_N^{(i)}$ are independent, but possibly correlated, draws from the distribution $p(AB\sigma_N|DI)$, that is, the result of the MCMC simulations above.

The posterior distribution for the number of cycles to failure is a weighted average (or mixture) of log normal distributions. Figure 8 shows the posterior distribution for the number of cycles to failure for a particular stress level (solid black line) and the equivalent distribution obtained using the best-fit parameter values (dashed blue line). The latter curve is a log normal distribution.

Usage Model

The usage model accounts for the variations in operating conditions of engines. The simplest approach assumes that each

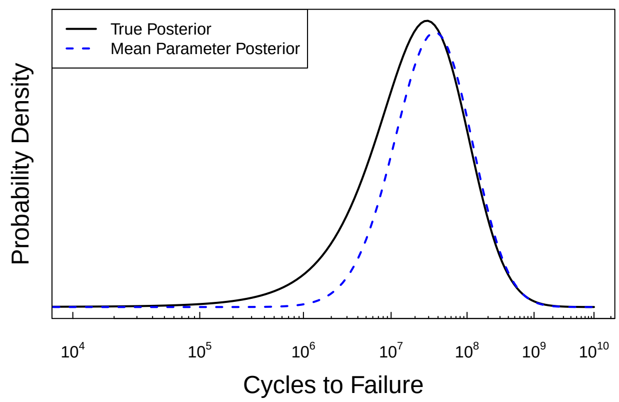

FIGURE 8. POSTERIOR DISTRIBUTION FOR THE NUMBER OF CYCLES TO FAILURE.

engine receives unlimited exposure at the worst possible flight condition. This is similar to Goodman-based approaches used today and it requires that a fatigue limit be defined. If the unlimited exposure model predicts an acceptable level of risk of fracture due to HCF, then no further work need be done.

For illustration, a simplified design mission (duty cycle) is considered. Full life is 25000 cycles (flights) and the usage is characterized by two duty cycles, an average flight and heavy, long-haul mission. The average flight profile is 1.7 engine flight hours in duration and occurs 85% of the time ($\approx$ 21250 cycles and 35870 EFH) while the heavy, long-haul profile is a 3 hour flight occurring the remaining 15% of the time ($\approx$ 3750 cycles and 11250 EFH). The mission profiles define all engine parameters, such as station temperatures, pressures and corrected rotor speeds.

Variation in sea-level ambient temperature at takeoff is modeled using a Gaussian distribution,

$$p(T_a|\mu_T,\sigma_T) = \frac{1}{\sqrt{2\pi}\sigma_T}\exp\left[-\frac{(T_a-\mu_T)^2}{2\sigma_T^2}\right] \tag{13}$$

with mean temperature $\mu_T = 68°$F and the standard deviation $\sigma_T = 25°$F. Combining the ambient takeoff temperature with the mission profile temperature variations defines the temperatures throughout the mission (specifically, the temperature parameter as required by Eqn. (4)).

The temperature-time history is combined with the time history of corrected rotor speed N_c to obtain mechanical speed for the mission from $N = N_c\sqrt{\frac{T}{T_{ref}}}$. Similarly, the resonant frequency versus time using Eqn. (2) and then the associated resonant crossing speed is calculated. Each resonant crossing in the mission is thus identified.

Damage Accumulation Model

The probabilistic analog to Miner's rule as described by Nelson [26, 27] is employed for damage accumulation modeling. In a deterministic approach, a stress level (typically the peak value) is associated with each passage through resonance. Additionally, a speed (or frequency) bandwidth is assumed, which, for single-degree-of-freedom (SDOF) responses, is a measure of the damping. These assumptions approximate the frequency response function by a square wave; when appropriate, more accurate SDOF approximations can be used. Combining the stress level and speed bin with the speed-time history curve, the exposure (or damage fraction) is

$$\varepsilon_i = \frac{\mathcal{N}_i}{\mathcal{N}_{0,i}} \tag{14}$$

where $\mathcal{N}_i$ is the calculated number of vibratory cycles accumulated and $\mathcal{N}_{0,i}$ is the median number of cycles to failure as given by Eqn. (10) during the i^{th} resonant crossing. The cumulative damage is

$$\varepsilon(N) = \frac{N_1}{N_{0,1}} + \frac{N_2-N_1}{N_{0,2}} + \cdots + \frac{N-N_{i-1}}{N_{0,i}} \tag{15}$$

and failure is assumed when $\varepsilon \geq 1$.

The probability model uses the same approximations to calculate the exposure ε (despite some obvious opportunities to quantify uncertainty). The difference from the deterministic approach is that rather than defining failure as a cumulative exposure that meets or exceeds 1.0, the exposure function is used to determine the probability of failure [26, 27] as

$$p(N|AB\varepsilon\sigma_N I) = \frac{\varepsilon'(N)}{\varepsilon(N)\sigma_N\sqrt{2\pi}}\exp\left\{-\frac{[\log\varepsilon(N)]^2}{2\sigma_N^2}\right\} \tag{16}$$

where $\varepsilon'(N) \equiv \frac{d\varepsilon}{dN} = 1/N_{0,k}$. The result is still a log normal distribution and equivalent to equation Eqn. (11) when the specimen is subjected to a single test. The exposure function $\varepsilon(N)$ is simply a device that modifies the probability distribution parameters to account for the changing dynamic stress.

Risk Calculation

Define the propositions

$$H_i \equiv \text{blade } i \text{ has fractured due to HCF.}$$

for $i = 1, 2, \ldots, N_b$ where N_b is the number of blades (18 in the present case). Then

$$p(H_i|\hat{N}AB\varepsilon\sigma_N I) = \int_0^{\hat{N}} p(N|AB\varepsilon\sigma_N I)dN \tag{17}$$

is the cumulative probability of fracture for a single blade through vibratory cycle $\hat{N}$ given the complete stress-time history as encoded by the exposure function $\varepsilon(N)$.

The requirements are specified on a per-stage basis, not a per-blade basis. Define the proposition

$$\begin{aligned} H_0 &\equiv \text{one or more blades in the stage has fractured} \\ &= H_1 + H_2 + \cdots + H_{N_b}. \end{aligned}$$

Then, the rules of probability theory give

$$p(H_0|\theta I) = 1 - \prod_{i=1}^{N_b} [1 - p(H_i|\theta I)] \tag{18}$$

as the probability of fracture due to HCF for the stage per engine lifetime (θ represents the conditioning parameters of Eqn. (17)). For very small individual blade risks $p(H_0|\theta I) \approx \sum p(H_i|\theta I)$. Dividing the result by the number of engine flight hours (EFH) yields a value appropriate for comparing to the allowable rates specified by the appropriate regulations.

The fleet risk is estimated as

$$R = \frac{1}{N_e} \sum_{k=1}^{N_e} r_k \tag{19}$$

where $r_k = p(H_0|\theta I)$ is the risk of failure for the k^{th} simulated engine. The value R is compared to the requirements to determine the acceptability of the design. Cruse and Brown [28] suggest that the risk R be acknowledged as uncertain. Using the samples r_k, the complete posterior distribution for knowledge of the HCF risk can be quantified and similarly the samples can also be used to define Bayesian credible intervals [7] of any desired size.

It is useful to also depict the simulation results graphically as shown in Fig. 9. For this hypothetical example, the red dot represents the maximum measured vibratory stress and the cloud of gray the maximum predicted vibratory stress for each of the simulated engines. The cloud can be thought of as what might have been reported on a Goodman diagram had different engines been tested.

In this example, the measured data point falls somewhat below the mean of the simulated values. This result is explained by the mistuning model which indicates that the IBR used to obtain the measured data is less responsive than typical.

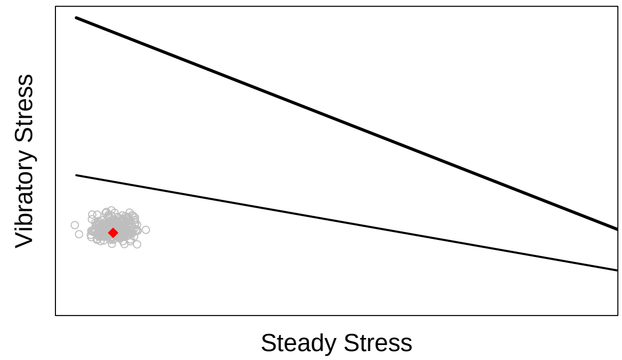

FIGURE 9. OVERLAY OF PROBABILISTIC HCF RISK ASSESSMENT SIMULATION DATA WITH LEGACY GOODMAN VALIDATION DATA.

CONCLUSIONS

A methodology for probabilistic HCF risk assessments based on Bayesian probability theory, in which probability distributions are used to encode uncertainty in states of knowledge, has been presented. The methodology was demonstrated via application to a simple integrally-bladed rotor using notional data from laboratory and rig testing. The demonstrated approach describes the implementation for engine validation and certification, but the same framework applies to the engine design and development phase (with suitable updates to the sub-models). The validation methodology is intended to be used for cases near to existing legacy Goodman criteria to better quantify the risk of HCF fracture. For designs well-below or well-above criteria, the legacy Goodman-based approach is a simple, prescriptive, and effective means of quantifying risk.

ACKNOWLEDGMENT

The authors would like to acknowledge Dr. Jeffrey Brown at the Air Force Research Laboratory Propulsion Directorate for his continuous support of applications of probabilistic HCF technologies.

REFERENCES

[1] Laplace, P.-S., 1996. *A Philosophical Essay on Probabilities*. Dover Publications. Original publication date 1814.

[2] Jeffreys, H., 2003. *Theory of Probability*, third ed. Oxford University Press.

[3] Cox, R. T., 1961. *The Algebra of Probable Inference*. The Johns Hopkins Press.

[4] Jaynes, E. T., 2003. *Probability Theory : The Logic of Science*. Cambridge University Press.

[5] Bretthorst, G. L., 1988. *Bayesian Spectrum Analysis and Parameter Estimation*. Springer-Verlag. `http://bayes.wustl.edu/glb/book.pdf`.

[6] Sivia, D., and Skilling, J., 2006. *Data Analysis: A Bayesian Tutorial*. Oxford University Press.

[7] Gregory, P. C., 2005. *Bayesian Logical Data Analysis for the Physical Sciences*. Cambridge University Press.

[8] Gilks, W., Richardson, S., and Spiegelhalter, D., 1996. *Markov Chain Monte Carlo In Practice*. Chapman & Hall/CRC, New York.

[9] Gelman, A., Carlin, J. B., Stern, H. S., and Rubin, D. B., 2003. *Bayesian Data Analysis*, second ed. Chapman & Hall/CRC.

[10] Gelman, A., and Hill, J., 2007. *Data Analysis Using Regression and Multilevel/Hierarchical Models*, second ed. Cambridge University Press.

[11] Liu, J. S., 2008. *Monte Carlo Strategies in Scientific Computing*. Springer.

[12] Collins, J. A., 1981. *Fatigue of Materials in Mechanical Design*. John Wiley & Sons.

[13] Tribus, M., 1969. *Rational Descriptions, Decisions and Designs*. Pergamon Press, Inc.

[14] DoD, 2002. *Military Handbook - MIL-HBDK-1783B: Engine Structural Integrity Program (ENSIP)*. U.S. Department of Defense.

[15] Federal Aviation Administration, 2010. *Title 14 – Aeronautics and Space, Part 33 Airworthiness Standards: Aircraft Engines*.

[16] Papalia, J., Lawless, P. B., and Fleeter, S., 2003. "CDA rotor generated unsteady aerodynamics of an upstream vane row". In 39th AIAA/ASME/SAE/ASEE Joint Propulsion Conference and Exhibit. Paper no. AIAA 2003-4980.

[17] Fulayter, R., 2004. "An experimental investigation of resonant response of mistuned fan and compressor rotors utilizing nsms". PhD thesis, Purdue University.

[18] Bretthorst, G. L., 1999. "The near-irrelevance of sampling frequency distributions". In Maximum Entropy and Bayesian Methods, W. von der Linden et al., eds., Kluwer Academic Publishers, pp. 21 – 46. `http://bayes.wustl.edu/glb/near-irrelevance.pdf`.

[19] Bretthorst, G. L., Hutton, W. C., Garbow, J. R., and Ackerman, J. J., 2005. "Exponential parameter estimation (in nmr) using bayesian probability theory". *Concepts in Magnetic Resonance,* ***27A***(2), pp. 55 – 63. `http://bayes.wustl.edu/glb/Given.pdf`.

[20] Robert, C. P., and Casella, G., 2007. *Monte Carlo Statistical Methods*. Springer.

[21] Meirovitch, L., 1986. *Elements of Vibration Analysis*. McGraw-Hill, Inc., New York.

[22] Whitehead, D. S., 1966. "Effect of mistuning on the vibration of turbomachine blades induced by wakes". *Journal of Mechanical Engineering Science,* ***8***, pp. 15–21.

[23] Whitehead, D., 1996. "The maximum factor by which forced vibration of blades can increase due to mistuning". In International Gas Turbine and Aeroengine Congress & Exhibition.

[24] Zellner, A., 1971. *An Introduction to Bayesian Inference in Econometrics*. Krieger.

[25] Plummer, M., 2003. "JAGS: A program for analysis of bayesian graphical models using gibbs sampling". In Proceedings of the 3rd International Workshop on Distributed Statistical Computing (DSC 2003).

[26] Nelson, W., 2001. "Prediction of field reliability of units, each under differing dynamic stresses, from accelerated test data". In *Handbook of Statistics*, N. Balakrishnan and C. R. Rao, eds., Vol. 20. Elsevier Science, pp. 611 – 621.

[27] Nelson, W. B., 2004. *Accelerated Testing, Statistical Models, Test Plans, and Data Analyses*. John Wiley & Sons, Inc., New York.

[28] Cruse, T. A., and Brown, J. M., 2007. "Confidence interval simulation for systems of random variables". *Transactions of the ASME,* ***129***, July, pp. 836 – 842.